
This is an electronic reprint of the original article.
This reprint may differ from the original in pagination and typographic detail.

Schön, Jonas; Vähänissi, Ville; Haarahiltunen, Antti; Schubert, Martin; Warta, Wilhelm; Savin, Hele

Main defect reactions behind phosphorus diffusion gettering of iron

Published in:
Journal of Applied Physics

DOI:
[10.1063/1.4904961](https://doi.org/10.1063/1.4904961)

Published: 01/01/2014

Document Version
Publisher's PDF, also known as Version of record

Please cite the original version:
Schön, J., Vähänissi, V., Haarahiltunen, A., Schubert, M., Warta, W., & Savin, H. (2014). Main defect reactions behind phosphorus diffusion gettering of iron. *Journal of Applied Physics*, 116(116).
<https://doi.org/10.1063/1.4904961>

This material is protected by copyright and other intellectual property rights, and duplication or sale of all or part of any of the repository collections is not permitted, except that material may be duplicated by you for your research use or educational purposes in electronic or print form. You must obtain permission for any other use. Electronic or print copies may not be offered, whether for sale or otherwise to anyone who is not an authorised user.

Main defect reactions behind phosphorus diffusion gettering of iron

Jonas Schön, Ville Vähänissi, Antti Haarahiltunen, Martin C. Schubert, Wilhelm Warta, and Hele Savin

Citation: *Journal of Applied Physics* **116**, 244503 (2014); doi: 10.1063/1.4904961

View online: <http://dx.doi.org/10.1063/1.4904961>

View Table of Contents: <http://scitation.aip.org/content/aip/journal/jap/116/24?ver=pdfcov>

Published by the [AIP Publishing](#)

Articles you may be interested in

[Competitive gettering of iron in silicon photovoltaics: Oxide precipitates versus phosphorus diffusion](#)

J. Appl. Phys. **116**, 053514 (2014); 10.1063/1.4892015

[Phosphorus and boron diffusion gettering of iron in monocrystalline silicon](#)

J. Appl. Phys. **109**, 093505 (2011); 10.1063/1.3582086

[Modeling phosphorus diffusion gettering of iron in single crystal silicon](#)

J. Appl. Phys. **105**, 023510 (2009); 10.1063/1.3068337

[Modeling boron diffusion gettering of iron in silicon solar cells](#)

Appl. Phys. Lett. **92**, 021902 (2008); 10.1063/1.2833698

[Experimental evidence for the presence of segregation and relaxation gettering of iron in polycrystalline silicon layers on silicon](#)

Appl. Phys. Lett. **85**, 4472 (2004); 10.1063/1.1819512



You don't still use this cell phone

or this computer

Why are you still using an AFM designed in the 80's?

It is time to upgrade your AFM

Minimum \$20,000 trade-in discount for purchases before August 31st

Asylum Research is today's technology leader in AFM

dropmyoldAFM@oxinst.com

OXFORD
INSTRUMENTS
The Business of Science®

Main defect reactions behind phosphorus diffusion gettering of iron

Jonas Schön,^{1,a)} Ville Vähänissi,² Antti Haarahiltunen,² Martin C. Schubert,¹ Wilhelm Warta,¹ and Hele Savin²

¹Fraunhofer Institute for Solar Energy Systems (ISE), Heidenhofstr. 2, 79110 Freiburg, Germany

²Aalto University, FI-00076 Aalto, Finland

(Received 17 October 2014; accepted 11 December 2014; published online 23 December 2014)

Phosphorus diffusion is well known to getter effectively metal impurities during silicon solar cell processing. However, the main mechanisms behind phosphorus diffusion gettering are still unclear. Here, we analyze the impact of oxygen, phosphosilicate glass as well as active and clustered phosphorus on the gettering efficiency of iron. The results indicate that two different mechanisms dominate the gettering process. First, segregation of iron through active phosphorus seems to correlate well with the gettered iron profile. Secondly, immobile oxygen appears to act as an effective gettering sink for iron further enhancing the segregation effect. Based on these findings, we present a unifying gettering model that can be used to predict the measured iron concentrations in the bulk and in the heavily phosphorus doped layers and explains the previous discrepancies reported in the literature. © 2014 AIP Publishing LLC. [<http://dx.doi.org/10.1063/1.4904961>]

I. INTRODUCTION

Phosphorus diffusion gettering (PDG) is an efficient and widely used technique to reduce the impact of metal impurities on the performance of silicon solar cells. However, the mechanisms that cause the redistribution of impurities from the bulk into the layers near the surface are still under research.

Gilles *et al.*¹ found that phosphorus doping increases the solubility of iron and thereby attracts impurities through segregation mechanisms. The increased solubility as a function of phosphorus concentration was explained by a Fermi-level effect and by the pairing of negatively charged substitutional iron with positively charged substitutional phosphorus.^{1,2} The presence of substitutional iron in heavily phosphorus doped silicon is supported also by the emission channeling patterns of Fe,³ by Mössbauer spectroscopy,^{4,5} and by *ab initio* calculations.^{6,7} In the PDG models previously reported, the segregation coefficient is based on the pairing of substitutional iron with substitutional phosphorus.^{2,8–12} However, the published segregation coefficients^{2,8–12} overestimate the segregation compared to the measurements of wafers from Ref. 1 with lower phosphorus concentrations than typically present in PDG experiments. Phang *et al.*¹³ recently revealed that a simple segregation mechanism based on an interaction of substitutional phosphorus and iron leads either to an underestimation of the gettering efficiency in heavily doped regions or to an overestimation in lowly doped regions, depending on the chosen segregation coefficient.¹³ Recent gettering experiments from Gindner *et al.*¹⁴ with phosphorus diffusions which result in the same sheet resistance but differ strongly in oxygen gas flow during drive-in support the finding that gettering cannot be solely explained by substitutional phosphorus.

In contrast to the models that are based on segregation of iron due to active phosphorus, Chen *et al.*^{15,16} and

Tryznadlowski *et al.*¹⁷ proposed a gettering mechanism that involves a complex of P₄V and Fe atoms. Their model was based on results of density functional theory (DFT) simulations¹⁶ and it was found to agree with the experiments reported in Ref. 11.

Syre *et al.*¹⁸ found a linear dependency between oxygen and iron profiles measured by SIMS in the heavily phosphorus doped layer. They explained the results with an iron oxygen vacancy complex. A quite similar effect of oxygen induced segregation of metals into the phosphorus doped layer was proposed by Amarray *et al.*¹⁹ Phosphosilicate glass (PSG) is discussed as another possible sink for iron.^{20,21}

To summarize, the proposed models explain single PDG experiment, but the exact gettering mechanism is still unclear. In this work, we aim to get a deeper insight into the dominating gettering mechanisms by analyzing a set of PDG experiments with a combination of SIMS and bulk iron measurements. We include experiments with varying concentration of inactive phosphorus, temperature and PSG thickness in order to separate the effect. We propose a model that is able to explain both the experiments reported previously and also the new results reported here.

II. EXPERIMENT

In the experiments, p-type Czochralski-grown silicon wafers with a thickness of 500 μm, a resistivity of 15.1–16.4 Ω-cm, and an oxygen level of 13 ppma ($6.5 \times 10^{17} \text{ cm}^{-3}$) were intentionally contaminated to two different iron levels: (i) $1.8 \times 10^{13} \text{ cm}^{-3}$ (low) and (ii) $1 \times 10^{14} \text{ cm}^{-3}$ (high). The contamination was done by a procedure which is described in more detail in Ref. 21. After contamination a 440-nm-thick oxide was grown on the wafers at 1000 °C. The high temperature treatment ensured a homogeneous Fe distribution throughout the wafer.²¹ Prior to phosphorus diffusion, the thermal oxide at the front side of the wafer was etched off. The backside oxide layer was kept as a diffusion barrier.

^{a)}email: jonas.schoen@ise.fraunhofer.de.

In order to study separately the impact of $\text{POCl}_3\text{-N}_2$ diffusion time and a low-temperature tail, four different phosphorus diffusion processes were applied (see Table I): (a) annealing at 870°C for 60 min in $\text{POCl}_3\text{-N}_2$ atmosphere with subsequent fast cooling (POCl60), (b) annealing at 870°C for 30 min in $\text{POCl}_3\text{-N}_2$ atmosphere + 30 min drive-in in an oxidizing atmosphere with subsequent fast cooling (POCl30_30), (c) annealing at 870°C for 60 min in $\text{POCl}_3\text{-N}_2$ atmosphere with subsequent slow cooling (1 h) to 800°C followed by 120 min at 800°C (POCl60+800) and (d) annealing at 870°C for 30 min in $\text{POCl}_3\text{-N}_2$ atmosphere + 30 min drive-in in an oxygen atmosphere with subsequent slow cooling (1 h) to 800°C followed by 120 min at 800°C (POCl30_30+800). During drive-in the ratio between oxygen and nitrogen is much higher than during the $\text{POCl}_3\text{-N}_2$ deposition phase. The resulting higher oxidation rates lead to higher silicon consumption and thicker glasses for processes with 30 min drive-in (see Table I).

After the phosphorus diffusion the phosphosilicate glass (PSG) at the front side of the wafer was etched off. Interstitial iron concentration in the wafer bulk was measured using the surface photovoltage (SPV) method by PV-2000 Semilab Inc. The measurement procedure is described in more detail in Ref. 21.

The phosphorus, oxygen, and iron profiles in the heavily doped regions were measured with secondary ion mass spectroscopy (SIMS). SIMS measurement was carried out either before or after the PSG was etched off, depending on the samples. In addition, depth profiles of the substitutional phosphorus concentrations were measured with electrochemical capacitance-voltage (ECV) profiling. The concentration of interstitial phosphorus is several orders of magnitude smaller than the substitutional phosphorus concentration. Thus, we can deduce the concentration of phosphorus in complexes and clusters from the difference of the SIMS and ECV results.

III. PROCESS SIMULATION

We use the software Sentaurus Process²² for the combined simulation of the PSG growth, phosphorus in-diffusion, oxygen in-diffusion, diffusion of silicon defects and iron gettering. The growth of the phosphosilicate glass (PSG) and the phosphorus in-diffusion during the POCl_3 process is based on the models presented in Ref. 23. The model considers the consumption of silicon during PSG growth. For the activation and clustering of phosphorus a transient model²² is used and all clustered phosphorus is assumed to be P_4V .

TABLE I. Summary of phosphorus diffusions, measured sheet resistances and glass thicknesses.

Process	POCl_3	Drive-in	800°C	R_{sheet}	Glass thickness
POCl60	60 min	—	—	24 Ω/sq	39 nm
POCl30_30	30 min	30 min	—	25 Ω/sq	75 nm
POCl60+800	60 min	—	120 min	21 Ω/sq	39 nm
POCl30_30+800	30 min	30 min	120 min	23 Ω/sq	75 nm

Silicon eigen defects, i.e., vacancies and interstitials of different charge states are simulated with the standard models of the software.²² The concentration of interstitials and vacancies at the silicon side of the PSG/Si interface is set to the solubility at the process temperature plus an extra interstitial flux depending on the reaction velocity of the PSG.

For the simulation of oxygen in-diffusion we assume two species to take the retardation of the oxygen diffusion in heavily phosphorus doped silicon^{24–26} into account: Interstitial oxygen (O_i) with the known diffusivity of $D(\text{O}_i) = 0.16 \times \exp\left(\frac{-2.529\text{eV}}{k_B T}\right) \text{cm}^2\text{s}^{-1}$ ²⁷ and an immobile oxygen species. In local equilibrium the ratio between the two species $k_{\text{immo}} = [\text{O}_{\text{immo}}]/[\text{O}_i]$ is constant. The effective oxygen diffusivity $D_{\text{eff}}(\text{O})$ in the heavily phosphorus doped layer can then be written as:

$$D_{\text{eff}}(\text{O}) = D(\text{O}_i) \times [\text{O}_i]/[\text{O}_{\text{Total}}] = D(\text{O}_i)/(1 + k_{\text{immo}}). \quad (1)$$

We assume that the PSG is an infinite source for oxygen that diffuses into the silicon. The oxygen concentration at the PSG/Si interface is given by:

$$[\text{O}_{\text{Total}}]_{\text{Interface}} = [\text{O}_i]_{\text{Interface}} \times (1 + k_{\text{immo}}). \quad (2)$$

k_{immo} and $[\text{O}_i]_{\text{Interface}}$ are fitted to the measured oxygen profiles.

Gettering of Fe is simulated with different segregation mechanisms for Fe, assuming local equilibrium. The value for the diffusivity of interstitial Fe in silicon is taken from Ref. 28. Gettered species are assumed to be immobile. The measured Fe concentrations before phosphorus diffusion are used as initial concentrations.

IV. RESULTS

A. Phosphorus profiles

Measured total phosphorus concentration profiles (SIMS) and substitutional phosphorus profiles (ECV) after POCl60 and POCl30_30 are shown in Figure 1. The two ECV profiles are rather similar: (i) There is a plateau at around $4 \times 10^{20} \text{cm}^{-3}$ in the first 80 (POCl30_30) to 90 nm

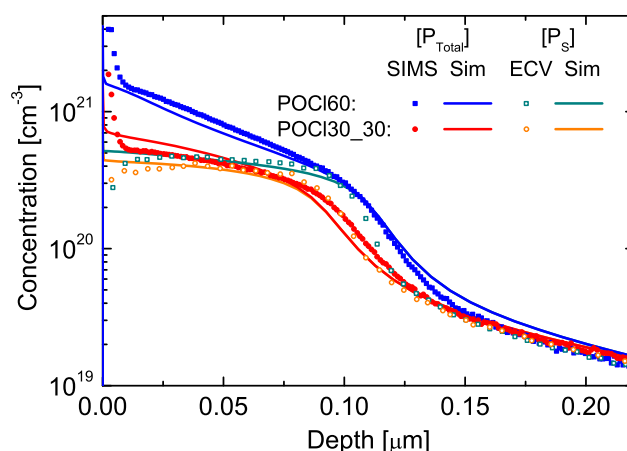


FIG. 1. Phosphorus profiles (SIMS and ECV) for processes POCl60 and POCl30_30 with the corresponding simulations.

(POCl60), which is only slightly higher after POCl60 and (ii) the overall profile depth is around 600 nm in both cases (slightly deeper after POCl30_30). On the contrary, the SIMS profiles differ significantly within the first 50 nm: The total phosphorus concentration after POCl60 is more than two times higher than after POCl30_30.

The simulated total and substitutional phosphorus profiles agree fairly well with the measured profiles (see Figure 1). Only the total phosphorus concentration for the POCl30_30 process is slightly overestimated in the simulations.

B. Oxygen profiles

Measured (SIMS) and simulated oxygen profiles after POCl30_30 + 800 and POCl60 + 800 processes are presented in Figure 2. The measured oxygen concentrations close to the PSG/Si interface are several orders of magnitude higher than the solubility of interstitial oxygen at the process temperature, given by $\text{Sol}(\text{O}_i) = 9 \times 10^{22} \text{ cm}^{-3} \times \exp\left(\frac{-1.52 \text{ eV}}{k_B T}\right)$.²⁷ In addition, the oxygen profiles indicate that the diffusivity in the heavily phosphorus doped region is approximately a factor of 1000 smaller than the diffusivity of interstitial oxygen in moderately doped silicon.²⁷ These observations could be explained by a second rather immobile oxygen species that is dominant in heavily phosphorus doped regions with high vacancy concentrations. In Refs. 24–26, a less pronounced retardation of the oxygen diffusion in phosphorus doped silicon is reported.

In this work, we cannot specify whether the immobile species is an oxygen dopant complex as proposed in Refs. 24 and 25, an oxygen vacancy complex^{29,30} or another oxygen complex. However, in the heavily phosphorus doped layer, the vacancy concentration is dominated by the concentration of the double negatively charged vacancies.^{31,32} Thus, the vacancy concentration is proportional to the quadratic electron concentration n : $[\text{V}^{2-}] \sim \left(\frac{n}{n_i}\right)^2 \times [\text{V}^0]$. The simulated concentration of neutral vacancies V^0 in the plateau region is almost identical for POCl60 and POCl30_30. The electron concentration n is determined by the active phosphorus concentration. Thus, the concentration of the rather immobile oxygen species increases with the electron concentration n in

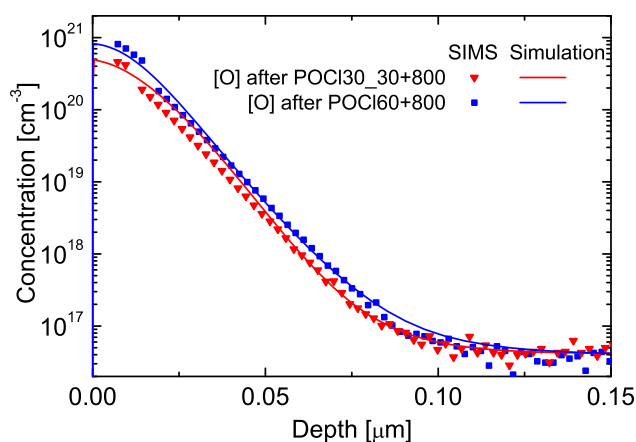


FIG. 2. Comparison of measured (SIMS) and simulated oxygen profiles after POCl30_30 + 800 and POCl60 + 800 processes.

both cases, with an oxygen vacancy and with an oxygen dopant complex.

By assuming that the immobile species is an oxygen vacancy complex, k_{immo} becomes proportional to n^2 . The concentration of neutral vacancies and other experimentally not easily accessible quantities are included in the fitted prefactor. The measured oxygen profiles are well reproduced with $k_{\text{immo}} = 0.09 \times \left(\frac{n}{n_i}\right)^2$ and an interstitial oxygen concentration at the interface of $[\text{O}_i]_{\text{Interface}} = 2 \times 10^{24} \text{ cm}^{-3} \times \exp\left(\frac{-1.52 \text{ eV}}{k_B T}\right)$ (see Figure 2). The interstitial oxygen concentration at the PSG/Si interface is a factor of 22 higher than the O_i solubility determined by Mikkelsen *et al.*²⁷ However, literature data for the oxygen solubility show considerable scatter.³³ One reason is that the oxygen surface concentration depends strongly on the processing condition and is higher during oxidation.^{33,34}

The dependency of the oxygen surface concentration on n ensures that the immobile species appears only in the heavily phosphorus doped region. The difference between the two oxygen profiles (Figure 2) is due to the dependency of the oxygen concentration at the PSG/Si interface on n and the higher silicon consumption during the drive-in phase (compared to the deposition phase) shifting the oxygen profile towards the PSG/Si interface.

C. Fe profiles

In Figure 3, the Fe profiles (a) are shown for highly and lowly contaminated samples after POCl60 + 800 and POCl30_30 + 800. The profiles have a maximum Fe concentration at the PSG surface and at the PSG/Si interface. The Fe profiles exhibit a steep decrease within the first 35–50 nm of silicon. During the next 60–80 nm, the Fe concentration decreases slightly until the detection limit of SIMS is reached. The POCl60 + 800 leads to higher Fe concentrations between 10 and 50 nm for the highly contaminated samples and to higher Fe concentrations after 40 nm for the lowly contaminated samples.

For all SIMS measurements, the overall Fe near the silicon surface (calculated from the SIMS profile) plus the measured bulk Fe concentration equals between 75% and 117% of the initial Fe content. The deviation of the Fe dose in silicon from the initial Fe dose is within the error margins of the SIMS measurements. In addition, lateral inhomogeneities of few percent in the P and O profiles should be taken into account. Within the limit of the measurement accuracy, we conclude that the dominant gettering takes place in the heavily phosphorus doped region. Nevertheless, high Fe concentrations were measured inside the PSG, especially towards the PSG surface. This may well be explained by indiffusion of Fe from the furnace. It is important to notice that our SIMS measurements give only qualitative profiles within the PSG because of the absence of a calibration standard.

D. Gettering mechanisms

For a first evaluation of the possible gettering mechanisms the depth profiles of the impurities that might cause the gettering of Fe are shown in Figure 3(b) below the measured Fe profiles (a). The ECV profiles for substitutional

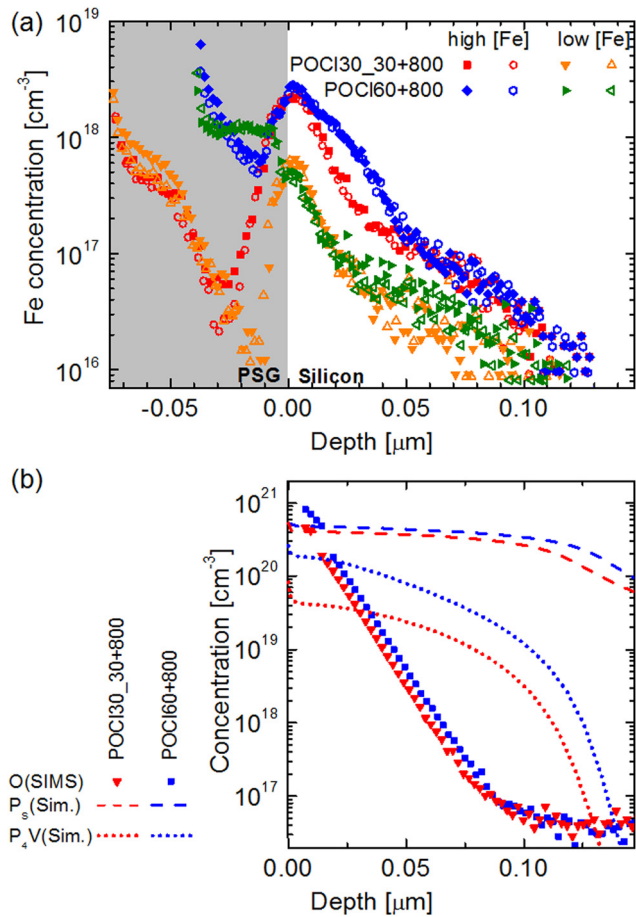


FIG. 3. Measured iron SIMS profiles (a), oxygen SIMS profiles (b), simulated active phosphorus (b) and simulated P_4V (b) after POCl30_30+800 and POCl60+800 processes. Filled and open symbols in (a) correspond to different SIMS measurements. Note that SIMS gives only qualitative Fe profiles within the PSG.

phosphorus have a typical slightly decreasing plateau in the first 110–130 nm determined by the phosphorus solubility. The profiles of the electron density, which might also influence the gettering effect (see Eq. (4)), have similar characteristics according to the simulations. The oxygen concentration decreases steeply from the interface towards the bulk and already after 60–70 nm reaches a typical oxygen concentration level found in silicon. The concentration of P_4V complexes decreases moderately in the first 100 nm. For the P_4V profiles, the largest difference can be seen between the wafers after POCl30_30+800 and POCl60+800 processes.

The shape of the Fe profiles from Figure 3(a) matches none of the profile shapes shown in (b). The steep decrease of the Fe profiles in the beginning correlates with the decrease of the oxygen concentration, but the smooth decrease between ~ 40 and ~ 120 nm follows the phosphorus profiles. Thus, the characteristics of the Fe curves can be explained by a superposition of 2 profiles suggesting that two separate mechanisms are responsible for the Fe gettering.

In the following, we simulate the PDG of Fe using combinations of different models to explain the experimental results. We start with the combination of an iron oxygen

complex and an interaction of substitutional Fe with substitutional phosphorus as in Refs. 2, 8, and 10.

We determine the segregation coefficient $k_{Fe}(O)$ for segregation of Fe into the surface layer due to high oxygen concentration as:

$$k_{Fe}(O) = \frac{[Fe_i]_{eq} + [FeO]_{eq}}{[Fe_i]_{eq}} = 1 + 1.9 \times 10^{-24} \text{cm}^3 \times \exp\left(\frac{1.9\text{eV}}{k_B T}\right) [O]. \quad (3)$$

For the simulation of segregation due to the interaction of substitutional phosphorus P^+ and Fe, we use the model presented in Ref. 10 with a segregation coefficient of:

$$k_{Fe}(P^+) = 1 + 1.0 \times 10^{-23} \text{cm}^3 \times \exp\left(\frac{0.51\text{eV}}{k_B T}\right) \times \left(\frac{n}{n_i}\right)^2 [P^+]. \quad (4)$$

The concentration of substitutional Fe and thus the segregation coefficient should be proportional to the vacancy concentration. However, the same argumentation as for the immobile oxygen species holds for the substitutional Fe: The vacancy concentration is dominated by the concentration of the double negatively charged vacancy which is proportional to n^2 . The concentration of neutral vacancies is included in the prefactor of the segregation coefficient. A dependency of the segregation coefficient on the experimentally inaccessible vacancy concentration is thus avoided.

Figure 4 shows the Fe profiles in the phosphorus doped region after POCl60_800 and POCl30_30_800 simulated with the combined model including both segregation mechanisms. After PDG, most of the Fe (>90%) is in the heavily phosphorus doped region. Thus, the total amount of Fe in this region can be increased only slightly (<10%) by process variation or a higher segregation coefficient. The simulated

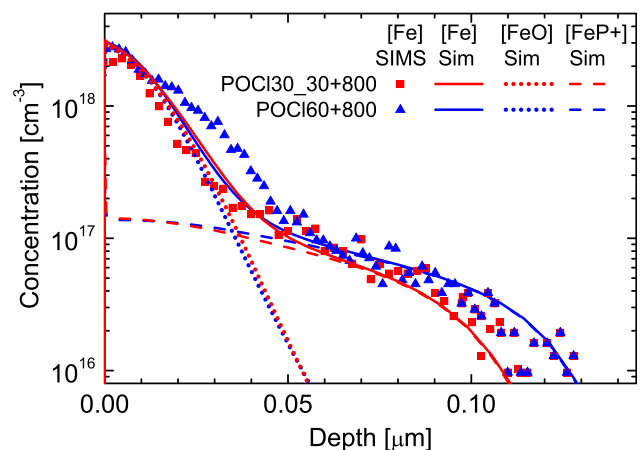


FIG. 4. Measured and simulated Fe profiles for POCl30_30+800 and POCl60+800 processes for high initial Fe concentrations. The used model considers segregation due to P^+ -Fe and Fe-O complexes. The dotted and dashed lines are simulated profiles of Fe gettering by the oxygen complex and the active phosphorus, respectively. For a clear presentation not all SIMS profiles from Figure 3(a) are shown.

Fe profiles agree well with the measured SIMS profiles. On the contrary, the shapes of the simulated Fe-O and Fe-P⁺ profiles (dotted and dashed lines in Figure 4) differ significantly from the SIMS Fe profiles. This demonstrates that gettering due to only one of the segregation mechanisms can be excluded. The height of the Fe profiles is determined by the chosen prefactor in the segregation coefficient equations (3) and (4). However, a different prefactor has no influence on the shape of the Fe profiles.

According to the simulations most of the Fe is gettered by the immobile oxygen complex. However, also the fraction of Fe gettered by substitutional phosphorus is significant.

The P₄V profiles in Figure 3(b) show a stronger decrease within the plateau region than the active phosphorus profiles. However, a P₄V complex would getter Fe mainly into the first 100–120 nm similar to the P⁺-Fe mechanism. Thus, we also implement a model considering Fe segregation due to Fe-O complexes and Fe-P₄V complexes.

As proposed in the model by Chen *et al.*,¹⁵ we assume a complex of P₄V-Fe with a binding energy of 1.52 eV. In our model, P₄V is the only complex for clustered phosphorus. We determine the pre-factor for the Fe-P₄V binding from our measurements. The segregation coefficient $k_s(P_4V)$ for regions with high P₄V concentrations is:

$$k_{Fe}(P_4V) = 1.0 + 2.9 \times 10^{-23} \text{cm}^3 \times \exp\left(\frac{1.52 \text{eV}}{k_B T}\right) \times [P_4V]. \quad (5)$$

The simulations for the combined model considering segregation due to Fe-O complexes and Fe-P₄V complexes are compared with the SIMS profiles in Figure 5. The correlation is almost as good as for the model considering segregation due to P⁺-Fe and Fe-O complexes (see Figures 4 and 5). The simulated P₄V-Fe concentrations are also shown in Figure 5. The results demonstrate that gettering due to only P₄V-Fe complexes cannot explain the measured Fe profiles.

Neither the combined model with P₄V-Fe and P⁺-Fe (Figure 5) nor the combined model with Fe-O and P⁺-Fe

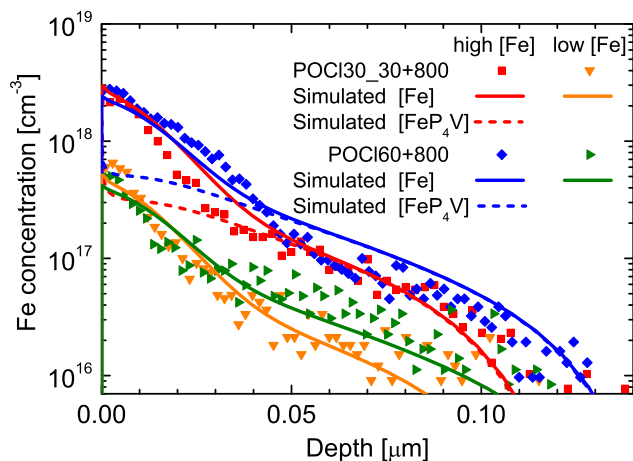


FIG. 5. Simulated Fe profiles for high and low initial [Fe] wafers after POC130_30 + 800 and POC160 + 800 processes in comparison to SIMS profiles. The used model considers segregation due to P₄V-Fe and Fe-O complexes. The dashed lines are simulated profiles of the Fe gettered by the P₄V complex.

(Figure 4) is able to reproduce the difference observed in the measured Fe profiles in the depth interval of 10–50 nm in POC130_30+800 and POC160 + 800 samples with high [Fe]. A similar difference is not observed in the low [Fe] samples (see Figure 5) that have a similar [Fe] shape (in the depth interval of 10–50 nm) as 'POC130_30 + 800' with high [Fe]. All other results, especially the Fe_i measurements (Figure 7), indicate that the gettering mechanisms are based on segregation which should result in similar Fe shapes for low and high [Fe]. Although further investigations are needed to judge if the observed difference is due to an additional mechanism, it is more likely resulting from small process variations or measurement uncertainties.

In addition, we test a combination of the segregation coefficients (4) and (5), i.e., P⁺-Fe complex and Fe-P₄V complex, but this combination is not able to reproduce the measured Fe profiles.

E. Interstitial Fe concentration

The detailed cooling process after phosphorus indiffusion is included in the simulations. During the cooling process, the Fe concentration at the front side decreases due to the increasing segregation coefficient (Eqs. (3)–(5)). Thus, the final Fe concentration is strongly inhomogeneous in depth. The simulated Fe_i concentration profile after POC160 + 800 using a cooling rate of 300 K/min outside the furnace is shown in Figure 6. For this Fe_i profile, we obtain a mean Fe_i concentration of $2.1 \times 10^{11} \text{cm}^{-3}$ in a distance between 5 and 9 μm from the front surface. This was experimentally confirmed by DLTS measurement where after of 5 μm silicon was etched off an Fe_i concentration of $2.2 \times 10^{11} \text{cm}^{-3}$ was measured.

In samples that have a low minority carrier lifetime, the SPV measurements are dominated by the carrier lifetime at the measurement side. Thus, the in depth inhomogeneity of the Fe_i profiles has to be considered when comparing the simulation and Fe_i concentration measurements in the bulk. We simulate the depth dependent electron density during the measurement with Sentaurus Device²² by assuming depth dependent diffusion length, which is calculated from the

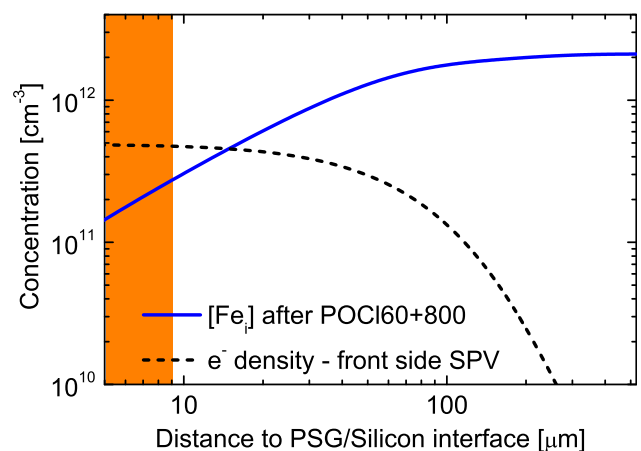


FIG. 6. Simulated Fe_i depth profile for a highly contaminated wafer after POC160 + 800 process and the simulated electron density during SPV measurement.

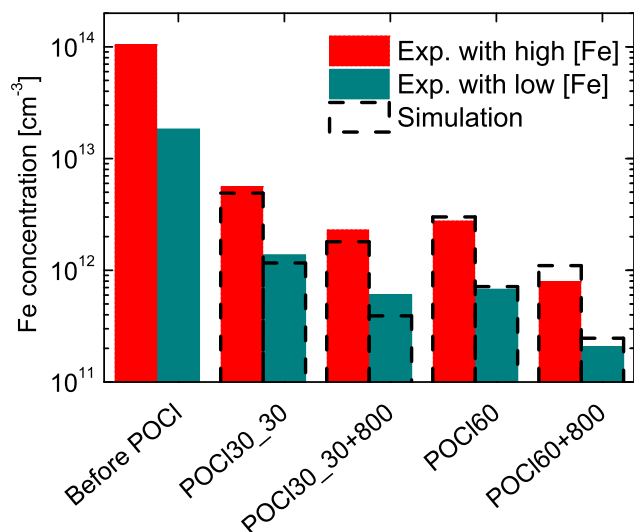


FIG. 7. Bulk Fe concentration after different processes measured using the surface photovoltage (SPV) technique.

simulated Fe_i depth profiles in the bulk (see Figure 6). From Figure 6, it becomes obvious that a direct comparison of simulated mean Fe_i concentration and SPV measurement from the front side leads to an overestimation of the segregation coefficient. Due to the inhomogeneous Fe_i concentration and the strong decrease of the electron density close to the surface, the measured Fe_i concentration depends strongly on the measurement side. Therefore, we simulate the electron density for the simulated Fe_i depth profiles and estimate the corresponding SPV signal by comparing the electron density with the results for homogeneous Fe_i concentrations. For highly contaminated wafers after POCl60 + 800 (see Figure 6), we simulate an Fe_i concentration of $2.0 \times 10^{12} \text{ cm}^{-3}$ (measurement: $2 \times 10^{12} \text{ cm}^{-3}$) for SPV from the backside and an Fe_i concentration of $1.2 \times 10^{12} \text{ cm}^{-3}$ (measurement: $0.8 \times 10^{12} \text{ cm}^{-3}$) for SPV from the front side. For higher Fe_i concentrations this effect becomes even more important. This effect was neglected in Ref. 11, which resulted in a systematically overestimated segregation coefficient (by about a factor of 1.5).

The simulated and measured Fe_i concentrations in Figure 7 determined from SPV from the front side coincide fairly well. An almost constant ratio between highly and lowly contaminated samples after different processes, i.e., the independence from total iron concentration, is another indication that no other mechanism than segregation, as reported in Ref. 21, is responsible for gettering. It is important to notice that while SIMS is unable to detect strong differences in gettering efficiency between 30 and 60 min POCl₃ (Figure 3(a)) the Fe_i concentration is clearly changing as seen in Figure 7.

Our proposed model is able to clarify the discrepancies in the published results on PDG. To give an example, the higher gettering efficiency of a short and strong P diffusion followed by an oxidation compared to a weak P diffusion with almost the same substitutional P profile¹³ is probably a result of the deeper oxygen profile. The relative small segregation effect found by Gilles *et al.*¹ in wafers doped with

phosphorus during crystallization can be explained if only the segregation due to phosphorus without the Fe-O complex is considered.

V. CONCLUSIONS

Conventionally, metal impurity gettering is characterized by measuring the remaining metal concentration in the wafer bulk which indeed is the measure of the actual gettering efficiency. However, in order to get a deeper insight on the actual gettering mechanisms, we have extended our study to characterize the iron profiles also in the heavily doped region after various phosphorus diffusion processes. Our findings support segregation based gettering by two parallel defect reactions: (i) between iron and immobile oxygen complex and (ii) between iron and phosphorus.

The SIMS profiles suggest that the segregation of Fe in heavily phosphorus doped regions is due to a reaction with active phosphorus. Thus, we propose a model including gettering due to the immobile oxygen complex and active phosphorus. However, a Fe-P₄V complex as proposed by Chen *et al.*¹⁵ (on the basis of DFT simulations) could not be fully excluded. Further experiments resulting in additional oxygen, phosphorus and substitutional phosphorus concentration data would be beneficial.

The presented model for PDG allows the simulation of iron gettering from the bulk together with accurate iron, phosphorus, and oxygen profiles in the heavily doped region. The new insights can be a promising basis for improving the gettering efficiency without influencing the emitter characteristics, e.g., using a process with similar sheet resistance but higher oxygen concentration in the vicinity of the surface.

ACKNOWLEDGMENTS

The authors would like to thank R. Müller for ECV measurements, P. Barth and H. Lautenschlager for processing, H. Steinkemper for help with device simulations, L. Mundt and J. Holtkamp for measurements of charge carrier lifetime, T. Mtchedlidze from Dresden University of Technology for the DLTS-measurements and S. Dunham from the University of Washington for fruitful discussions about PDG mechanisms. Authors from Aalto University acknowledge the funding from Academy of Finland and Finnish National Technology Agency.

¹D. Gilles, W. Schröter, and W. Bergholz, *Phys. Rev. B* **41**(9), 5770–5782 (1990).

²S. M. Myers, M. Seibt, and W. Schröter, *J. Appl. Phys.* **88**(7), 3795–3819 (2000).

³D. J. Silva, U. Wahl, J. G. Correia, and J. P. Araújo, *J. Appl. Phys.* **114**, 103503 (2013).

⁴G. Weyer, A. Burchard, M. Fanciulli, V. N. Fedoseyev, H. P. Gunnlaugsson, V. I. Mishin, and R. Sielemann, *Physica B* **273–274**, 363–366 (1999).

⁵Y. Yoshida, S. Aoki, K. Sakata, Y. Suzuki, M. Adachi, and K. Suzuki, *Physica B* **401–402**, 119 (2007).

⁶S. K. Estreicher, M. Sanati, and N. Gonzalez Szwacki, *Solid State Phenom.* **131–133**, 233–240 (2008).

⁷S. K. Estreicher, M. Sanati, and N. Gonzalez Szwacki, *Phys. Rev. B* **77**, 125214 (2008).

⁸A. Haarhiltunen, H. Savin, M. Yli-Koski, H. Talvitie, and J. Sinkkonen, *J. Appl. Phys.* **105**(2), 023510–023514 (2009).

- ⁹B. Michl, J. Schön, W. Warta, and M. C. Schubert, *J. Photovolt.* **3**, 635–640 (2013).
- ¹⁰J. Schön, M. C. Schubert, W. Warta, H. Savin, and A. Haarahiltunen, *Physica Status Solidi A* **207**(11), 2589–2592 (2010).
- ¹¹H. Talvitie, V. Vähänissi, A. Haarahiltunen, M. Yli-Koski, and H. Savin, *J. Appl. Phys.* **109**, 093505 (2011).
- ¹²J. Hofstetter, D. P. Fenning, M. I. Bertoni, J.-F. Lelièvre, C. del Cañizo, and T. Buonassisi, *Prog. Photovolt.* **19**, 487 (2011).
- ¹³S. P. Phang and D. Macdonald, *IEEE J. Photovolt.* **4**, 64–69 (2014).
- ¹⁴S. Gindner, P. Karzel, B. Herzog, and G. Hahn, *IEEE J. Photovolt.* **4**(4), 1063–1070 (2014).
- ¹⁵R. Chen, B. Trzynadlowski, and S. T. Dunham, *J. Appl. Phys.* **115**, 054906 (2014).
- ¹⁶R. Chen, Ph.D. thesis, University of Washington, 2012.
- ¹⁷B. Trzynadlowski, A. Yazdani, R. Chen, and S. T. Dunham, in Proceedings of the 38th IEEE Photovoltaic Specialists Conference, p. 1584 (2012).
- ¹⁸M. Syre, S. Karazhanov, B. R. Olaisen, A. Holt, and G. Svensson, *J. Appl. Phys.* **110**, 024912 (2011).
- ¹⁹E. Amarray and J. P. Deville, *Rev. Phys. Appl.* **22**, 663–669 (1987).
- ²⁰J. Schön and W. Warta, in Proceedings of the 23rd European Photovoltaic Solar Energy Conference, Valencia, Spain, p. 1851 (2008).
- ²¹V. Vähänissi, A. Haarahiltunen, H. Talvitie, M. Yli-Koski, and H. Savin, *Prog. Photovolt: Res. Appl.* **21**, 1127–1135 (2013).
- ²²Synopsys, *Sentaurus™ User Guide, release H-2013.03* (Zurich, Switzerland, 2013).
- ²³J. Schön, A. Abdollahinia, R. Müller, J. Benick, M. Hermle, W. Warta, and M. C. Schubert, *Energy Procedia* **38**(0), 312–320 (2013).
- ²⁴H. Takeno, K. Sunakawa, and M. Suezawa, *Appl. Phys. Lett.* **77**, 376 (2000).
- ²⁵C. Gao, Z. Wang, X. Liang, D. Tian, H. Liu, X. Ma, and D. Yang, *J. Phys.: Condens. Matter* **24**(49), 495802 (2012).
- ²⁶D. Timerkaeva, D. Caliste, and P. Pochet, *Appl. Phys. Lett.* **103**, 251909 (2013).
- ²⁷J. C. J. Mikkelsen, in Materials Research Society Symposia Proceedings, Boston, USA, p. 19 (1988).
- ²⁸A. A. Istratov, H. Hieslmair, and E. R. Weber, *Appl. Phys. A* **69**(1), 13–44 (1999).
- ²⁹J. W. Corbett, G. D. Watkins, and R. S. McDonald, *Phys. Rev.* **135**, A1381 (1964).
- ³⁰J. L. Lindstrom, L. I. Murin, V. P. Markevich, T. Hallberg, and B. G. Svensson, *Physica B* **273–274**, 291–295 (1999).
- ³¹A. Bentzen, A. Holt, J. S. Christensen, and B. G. Svensson, *J. Appl. Phys.* **99**, 064502 (2006).
- ³²R. B. Fair and J. C. C. Tsai, *J. Electrochem. Soc.* **124**(7), 1107–1118 (1977).
- ³³P. Pichler, *Intrinsic Point Defects, Impurities, and Their Diffusion in Silicon* (Springer, Wien, 2004), p. 471.
- ³⁴J. C. J. Mikkelsen, *Appl. Phys. Lett.* **41**(9), 871–873 (1982).